Bone regeneration by the osteoconductivity of porous titanium implants manufactured by selective laser melting: A histological and micro computed tomography study in the rabbit

de Wild, Michael ; Schumacher, Ralf ; Mayer, Kyrill ; Schkommodau, Erik ; Thoma, Daniel ; Bredell, Marius ; Kruse Gujer, Astrid ; Grätz, Klaus W ; Weber, Franz E

Abstract: The treatment of large bone defects still poses a major challenge in orthopaedic and cranio-maxillofacial surgery. One possible solution could be the development of personalized porous titanium-based implants that are designed to meet all mechanical needs with a minimum amount of titanium and maximum osteopromotive properties so that it could be combined with growth factor-loaded hydrogels or cell constructs to realize advanced bone tissue engineering strategies. Such implants could prove useful for mandibular reconstruction, spinal fusion, the treatment of extended long bone defects, or to fill in gaps created on autograft harvesting. The aim of this study was to determine the mechanical properties and potential of bone formation of light weight implants generated by selective laser melting (SLM). We mainly focused on osteoconduction, as this is a key feature in bone healing and could serve as a back-up for osteoinduction and cell transplantation strategies. To that end, defined implants were produced by SLM, and their surfaces were left untreated, sandblasted, or sandblasted/acid etched. In vivo bone formation with the different implants was tested throughout calvarial defects in rabbits and compared with untreated defects. Analysis by micro computed tomography (μCT) and histomorphometry revealed that all generatively produced porous Ti structures were well osseointegrated into the surrounding bone. The histomorphometric analysis revealed that bone formation was significantly increased in all implant-treated groups compared with untreated defects and significantly increased in sand blasted implants compared with untreated ones. Bone bridging was significantly increased in sand blasted acid-etched scaffolds. Therefore, scaffolds manufactured by SLM should be surface treated. Bone augmentation beyond the original bone margins was only seen in implant-treated defects, indicating an osteoconductive potential of the implants that could be utilized clinically for bone augmentation purposes. Therefore, designed porous, lightweight structures have potential for bone regeneration and augmentation purposes, especially when complex and patient-specific geometries are essential.

DOI: https://doi.org/10.1089/ten.TEA.2012.0753

DOI: https://doi.org/10.1089/ten.TEA.2012.0753

TISSUE ENGINEERING: Part A
Volume 00, Number 00, 2013

DOI: 10.1089/ten.tea.2012.0753

Original Article

Bone Regeneration by the Osteoconductivity of Porous Titanium Implants Manufactured by Selective Laser Melting: A Histological and Micro Computed Tomography Study in the Rabbit

Michael de Wild, PhD,[1] Ralf Schumacher, BSc,[1] Kyrill Mayer, BSc,[1] Erik Schkommodau, PhD,[1] Daniel Thoma, DDS,[2] Marius Bredell, MD, DDS,[3] Astrid Kruse Gujer, MD, DDS,[3] Klaus W. Grätz, MD, DDS,[3] and Franz E. Weber, PhD[3,4]

The treatment of large bone defects still poses a major challenge in orthopaedic and cranio-maxillofacial surgery. One possible solution could be the development of personalized porous titanium-based implants that are designed to meet all mechanical needs with a minimum amount of titanium and maximum osteopromotive properties so that it could be combined with growth factor-loaded hydrogels or cell constructs to realize advanced bone tissue engineering strategies. Such implants could prove useful for mandibular reconstruction, spinal fusion, the treatment of extended long bone defects, or to fill in gaps created on autograft harvesting. The aim of this study was to determine the mechanical properties and potential of bone formation of light weight implants generated by selective laser melting (SLM). We mainly focused on osteoconduction, as this is a key feature in bone healing and could serve as a back-up for osteoinduction and cell transplantation strategies. To that end, defined implants were produced by SLM, and their surfaces were left untreated, sandblasted, or sandblasted/acid etched. *In vivo* bone formation with the different implants was tested throughout calvarial defects in rabbits and compared with untreated defects. Analysis by micro computed tomography (μCT) and histomorphometry revealed that all generatively produced porous Ti structures were well osseointegrated into the surrounding bone. The histomorphometric analysis revealed that bone formation was significantly increased in all implant-treated groups compared with untreated defects and significantly increased in sand blasted implants compared with untreated ones. Bone bridging was significantly increased in sand blasted acid-etched scaffolds. Therefore, scaffolds manufactured by SLM should be surface treated. Bone augmentation beyond the original bone margins was only seen in implant-treated defects, indicating an osteoconductive potential of the implants that could be utilized clinically for bone augmentation purposes. Therefore, designed porous, light-weight structures have potential for bone regeneration and augmentation purposes, especially when complex and patient-specific geometries are essential.

Introduction

Surgeons are in an on-going search for the ideal solution for bridging larger bony defects in the facial and nonfacial skeleton. Titanium foams tested *in vitro* with human osteoblasts have shown osteoblast colonization and differentiation into mature bone cells, and, consequently, belong to suitable bone substitute materials in mechanically demanding sites.[1] Porous titanium scaffolds with a homogeneous pore size distribution can be produced by means of powder metallurgy or CVD coating of vitreous carbon scaffolds.[2,3] Metal injection methods[4] allow forming porous foams with open porosity by means of NaCl as placeholders.[5] The water-soluble placeholders, however, are randomly distributed. Therefore, with all these methods it is impossible to define the location and size of dedicated micrometre-size channels, gradients or

[1]Institute for Medical and Analytical Technologies, School of Life Sciences, University of Applied Sciences Northwestern Switzerland, Muttenz, Switzerland.
[2]Center for Dental Medicine, Clinic of Fixed and Removable Prosthodontics and Dental Material Science, University of Zurich, Zurich, Switzerland.
[3]Division of Cranio-Maxillofacial and Oral Surgery, Oral Biotechnology & Bioengineering, University Hospital, Zurich, Switzerland.
[4]Zurich Center for Integrative Human Physiology (ZIHP), University of Zurich, Zurich, Switzerland.

patterns. In addition, in all these architectures, the special distribution of the pores is mainly unsystematic and unplanned,[6] and the exact porous structure is not reproducible.

Additive manufacturing (AM, formerly referred to as Rapid Manufacturing) is a layer-by-layer production method that allows production of simple[7] as well as complex-shaped structures based on computer-aided design (CAD) data sets.[8–10] Laser-based AM processes (selective laser melting [SLM]) allow the production of bone implants made of metals such as titanium and titanium-based alloys[8,11–15] with an exactly defined strut size as small as 200 μm.[16]

Biomaterial-tissue interactions and bone healing[17] are dependent on the chemistry and topography of the artificial material.[14,18–22] A rough sandblasted and acid-etched surface, for example, enhances the proliferation of bone cells and stimulates the secretion of the extra cellular matrix.[15] A sandblasted and acid-etched surface, one of the most effective artificial surface structures on commercially pure titanium to be accepted by bony tissue, is based on a moderately rough topography.[23] This binary procedure of the so-called sandblasted and acid-etched surface leads to a fast osseointegration, for example, with dental implants.[12,24,25] It was shown *in-vitro* that SLM-fabricated structures with native, sandblasted and acid-etched, sandblasted, polished, or vibratory grinded surfaces show an identical cytocompatibility compared with conventional titanium surfaces.[26]

The final aim of the overall project is to generate defined scaffolds by SLM for the treatment of large bone defects to be used in conjunction with growth factor-loaded hydrogels or cell constructs for bone tissue engineering. In this initial study, we evaluated the mechanical properties, osteoconduction, and bone augmentation properties of defined titanium-based open porous scaffolds produced by SLM used as a bone substitute in calvarial defects in rabbits, and compared them with untreated defects.

Materials and Methods

Implant design and production

The titanium structures for this study were designed with Software Solidworks (www.solidworks.com) and Magics (www.materialise.com), as displayed in Figure 1a. The implants have an open-porous lattice and a stepped cylindrical shape with an upper outer diameter of 7.5 mm, a lower outer diameter of 6 mm, and a height of 3.8 mm. The rod thickness was set to 200 μm. The open porous channels with a quadratic cross section of 700×700 μm are designed in an orthogonal arrangement with an overall porosity of 83.5%. The designed surface area of the model is 411.5 mm^2, whereas the enwrapping stepped cylinder has a surface of 169.0 mm^2, that is, 2.4 times smaller.

The implants were produced with the SLM Realizer 100 SLM machine (SLM Solutions) as displayed in Figure 1b and operated with a continuous wave Ytterbium-fibre laser with a wavelength between 1068 and 1095 nm. The raw material was Ti-powder (Ti grade II according to ASTM F67, 20–63 μm particle size; SLM Solutions) with a d_{50}-value of 30 μm. The laser parameters were adjusted to an energy density E_v of 63 J/mm^3. After fabrication (Fig. 1c), the samples were cleaned from adhering powder particles by compressed air and ultrasonic treatment. For reasons of handling during production and implantation, a transfer pin is connected to the implant via a predetermined breaking point (Fig. 1c).

Evaluation of the mechanical properties of the implant material

The mechanical properties of the structures were determined in a universal material testing machine (Zwick Roell 100kN) under uniaxial compressive load. The implants were placed horizontally, lying between two hard metal compression inserts simulating the biomechanical loading on the

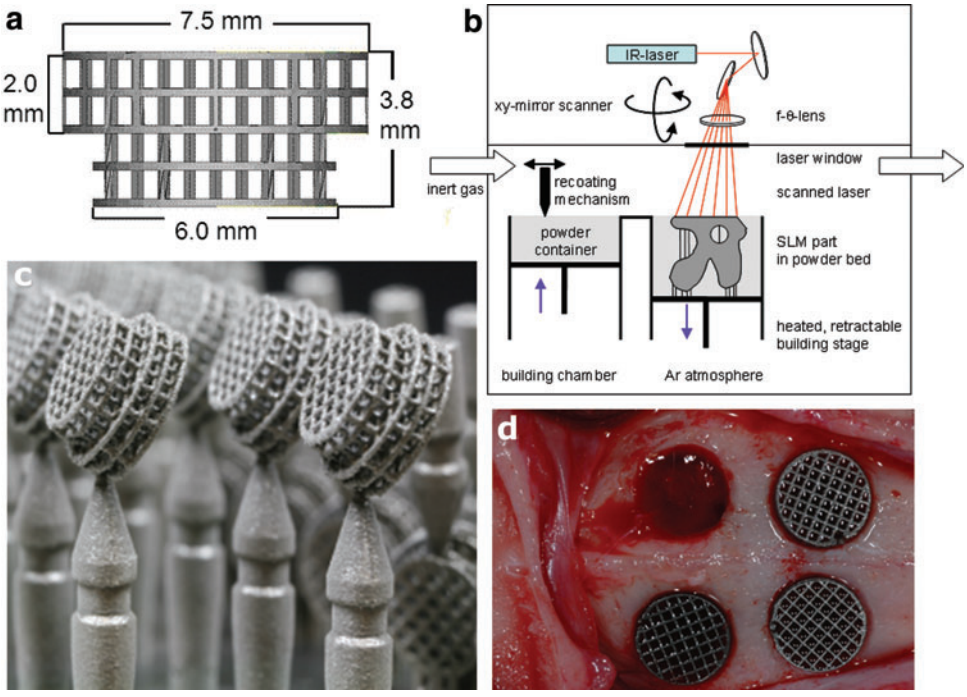

FIG. 1. SLM process and implant design. **(a)** Implant design, including lattice dimension. **(b)** Schema of the SLM process. Metal powder is locally melted by an intensive infrared laser beam (100cW TEM00) that traces the layer geometry (down to 30 μm layer thickness), www.slm-solutions.com. **(c)** Photograph of implants on the building platform supported on a transfer pin after excavation from the powder. **(d)** Intraoperative situation: three implants and an empty craniotomy defect. SLM, selective laser melting. Color images available online at www.liebertpub.com/tea

scaffolds during and after the operation. The force and deformation were recorded during the strain-controlled compression phase with a constant strain of $0.001\,s^{-1}$ at room temperature.

Surface modification and analysis

Three different types of implant surfaces were used in this study: (1) native SLM, (2) sandblasted, and (3) sandblasted and acid-etched surfaces. The latter two types were blasted with corundum particles MS-EKR80A at 5 bar for 60 s on a PEENMATIC 620S (IEPCO AG). Subsequently, the samples were treated in a hot mixture of acid HCl (32%; Fluka): H_2SO_4 (95%; J.T. Baker): ultrapure H_2O (resistivity 18.2 MΩcm, ELGA Purelab Option-Q DV 25) (2:1:1 v/v) at 93°C for 15 min and then rinsed thrice with ultrapure water (resistivity 18.2 MΩcm) in an ultrasonic bath.

Two-dimensional (2D) and three-dimensional (3D) surface roughness were analyzed according to EN ISO 4287:1998 and ISO 13565-2:1996-12 standards. Three roughness values were experimentally determined by Confocal Laser Scanning Microscope (Olympus Lext OLS 3100) with a 50× objective. An area of 100×100 μm was analyzed at the intersection points of the lattice. The evaluation of the height descriptive roughness parameters Sra, SRq, and SRz and the spatial roughness parameter RSm and Rku was done with a cut-off wavelength of $\lambda = 1/10$ Lo = 10 μm.

The surface morphology and chemistry were analyzed by scanning electron microscopy (SEM, Hitachi TM-1000, 15 kV, Solid State Backscattered Electron Detector) equipped with an energy dispersive X-ray spectrometer (EDX, SwiftED-TM detector, Na11–U92).

Sample preparation

All samples were ultrasonically cleaned in a 4% Deconex® 15PF (Beiersdorf) solution at 90°C for 5 min, then cleaned thrice in ultrapure water (resistivity 18.2 MΩcm) for 15 min in an ultrasonic bath, and twice passivated in concentrated nitric acid (65% HNO_3; Fluka) under ultrasonic agitation. Before packaging, the samples were cleaned and sterilized in high purity oxygen RF plasma (PDC-32G; Harrick, oxygen purity 99.9995%, Carbagas) at 29.7 W for 5 min. The SLA samples were packed under inert argon atmosphere in a sealed vial filled with sterile 0.9% NaCl solution. Samples with the native SLM surface and sandblasted SLM surface were packed in empty vials. All vials were then sealed in sterilization bags. Before the *in-vivo* tests, the samples underwent gamma sterilization with 25 kGy.

Surgical procedure

Five adult (12 months old) New Zealand White rabbits, weighing between 3 and 4 kg, were used in the present study. The animals were kept in a purpose-designed room for experimental animals and were fed a standard laboratory diet. The study was evaluated and accepted by the responsible Veterinary Authority of the Kanton Zurich. Animals were anesthetized by an injection of 65 mg/kg ketamine and 4 mg/kg xylazine, and maintenance was with isofluoran/O_2. The surgical area was disinfected, and a straight incision was made from the nasal bone to the midsagittal crest. The soft tissues were reflected, and the periosteum was elevated from the site. In the area of the right and left parietal and frontal bones, four evenly distributed 6 mm diameter craniotomy defects were prepared with a trephine bur under copious irrigation with sterile saline. Care was exercised to avoid injury of the dura. The surgical area was flushed with saline to remove bone debris. Each of the animals received all four different treatment modalities: empty, (1) native SLM implant, (2) sandblasted SLM implant, and (3) sandblasted and acid-etched SLM implant (Fig. 1d). The treatment modalities were assigned at random for the first animal and thereafter, cyclic permuted clockwise for the next three animals. For the fifth animal, treatment modalities were again assigned at random. After carefully placing the implants into the defects, the soft tissues were closed with interrupted sutures. After a healing period of 8 weeks, the rabbits were sacrificed by an overdose of ketamine. The skull containing all four craniotomy sites was removed and placed in 40% ethanol.

Embedding

The specimens were prepared with a sequential water substitution process that involved 48 h in 40% ethanol, 72 h in 70% ethanol (changed every 24 h), 72 h in 96% ethanol, and, finally, 72 h in 100% ethanol. The samples were then placed in xylene for 72 h (changed every 24 h). Next, the samples were infiltrated by placing them in methyl methacrylate (MMA) for 72 h (Fluka 64200) followed by 3 days in 100 mL MMA + 2 g di-benzoylperoxid (Fluka 38581) at 4°C. Samples were embedded by placing them in 100 mL MMA + 3 g di-benzoylperoxid + 10 mL plastoid N or dibutyl phthalate (Merck 800 19.25) and allowing polymerization to occur at 37°C in an incubator. After embedding, the skull was cut in four pieces each containing one craniotomy site by using an Exakt 300P saw (Exakt).

μCT analysis

Hard tissue and implant material distribution in the embedded, separated craniotomy sites were determined by a SkyScan 1172™ high-resolution μCT scanner (SkyScan NV), equipped with a 100 kV/100 μA X-ray source and a 10-megapixel X-ray-sensitive CCD camera. The flat samples were rotated around the vertical symmetry axis in steps of 0.4° with the circular closing rings in horizontal orientation, see Figure 1a. The specimens were individually 360°-scanned using an accelerating voltage of 100 kV and a beam current of 100 μA, resulting in 900 projection images. A 0.5 mm Al filter was used to increase the mean photon energy. The reconstruction was carried out by the cluster-based NRecon software (Version 1.4.4; SkyScan NV), which distributed the calculation parallel to five computers. The reconstruction leads to a set of 937 stacked slices with a dynamic range of 8 bit. The morphological analysis was done with the CTAn software (version 1.8.0.5; SkyScan NV).

Histology

After μCT analysis, embedded craniotomy sites were sectioned by a diamond band saw (Exakt 300P) in the middle of the defect, glued to a support, and sectioned again, so that a 200 μm-thick sample from the middle was attached to the

support. The thickness of this sample was further reduced to 40–60 μm by a grinding machine (Exakt 420 CS). To visualize tissues, the samples were surface stained by toluidine blue. Digital images were taken and processed with an image analysis program (Adobes Photoshop CS3). Quantitative evaluation of bone regeneration was done by applying standard morphometrical techniques as reported earlier.[27,28]

Bone bridging

Bone bridging was determined in the middle section. First, the areas with bone tissue were projected onto the x-axis. Next, the stretches of the x-axis where bone formation had occurred at any level were summed up as described earlier.[27,28] Bone bridging is given in percentage of the defect width (6 mm) where bone formation has occurred.

Statistical analysis

The primary analysis unit was the animal. For all parameters tested, the four treatment modalities were compared with a Friedman test, followed by pairwise comparison of treatment modalities with the Wilcoxon-signed rank test for dependent data (IBM SPSS v.19). p-values for the probability of significant differences between treatments are displayed in the graphs, and significance was set at $p < 0.05$. Data from five rabbits are presented. Values are reported as mean ± SD and displayed as box plots ranging from the 25th (lower quartile) to the 75th (upper quartile) percentile, including the median and whiskers showing the minimum and maximum values.

Results

Process and implant characterization

In order to qualify the production process, the produced SLM pieces were compared with the structure virtually defined in CAD. The geometric differences detected between the CAD model and materialized physical implants are mainly in the strut size: The planned CAD strut size of 200 μm was found to be 238 ± 29 μm for the as-produced implants with native surface. The pore sizes of the native implants have a size of 578 ± 27 μm. The strut size of the sandblasted implants is 212 ± 27 μm, with pore sizes of 642 ± 37 μm. Surface treatment by sandblasting and acid etching changes the elemental composition from 99.75% Ti to 90.5% Ti and 9.5% Al due to corundum particles that stick to the surface and are not removed by ultrasonic cleaning. After the acid etching, most of the Al_2O_3 particles are detached, and the amount of Al on the surface composition is reduced to 1%. These surface treatments also reduce the surface roughness SR_a of the native SLM implant from 3.33 ± 0.27 to 0.94 ± 0.07 μm for sandblasted surface and to 1.16 ± 0.11 μm for the sandblasted and acid-etched surface (Table 1). The Confocal Laser Scanning Microscopic analysis assessed that the amplitude roughness parameters and spatial roughness parameters were reduced on surface modification. Furthermore, the effective surface area of the native topography is reduced by the treatments: The native surface shows a surface area ratio Sdr of 2.64 (i.e., ratio between the effective surface and the projected area), whereas the sandblasted surface is reduced to Sdr = 1.44 and the sandblasted and acid-etched surface is reduced to Sdr = 1.76.

Table 1. Surface Roughness Parameters Depending on the Chemical and Mechanical Surface Modifications

Roughness parameter [μm]	*SLM native*	*Sandblasted*	*SLA*
SRa	3.33 ± 0.27	0.94 ± 0.07	1.16 ± 0.11
SRq	4.41 ± 0.34	1.22 ± 0.08	1.53 ± 0.22
SRz	46.87 ± 4.22	11.88 ± 1.20	16.00 ± 3.78
RSm	12.79 ± 3.80	10.16 ± 1.93	7.70 ± 0.84
Rku	3.70 ± 1.08	3.43 ± 1.17	2.86 ± 0.42

Values are averages over $n = 6$ for each surface.
Roughness amplitude parameters: SRa, arithmetic mean deviation of the surface; SRq, root-mean-square deviation of the surface; SRz, peak to valley height.
Roughness spacing parameters: RSm, mean line peak spacing.
Roughness amplitude distribution parameters: Rku, surface kurtosis.
SLA, sand blasted acid-etched; SLM, selective laser melting.

The change in the surface topography is also evident in representative SEM pictures taken from the different implant types (Fig. 2). The native SLM surface (left) is covered by spherical particles from the starting powder material that are not fully melted but only sintered to the implant. The sandblasted surface (center) exhibits a flaked topography arising from the abrasive blasting process. The sandblasted and acid-etched surface (right) is characterized by a superposition of cavities with a diameter of roughly 50 μm from the sandblasting with pits of diameter 1–2 μm from the acid-etching process.

Static compression tests of the implants ($n = 5$) resulted in a compressive strength of $R_m = 15.9 \pm 0.4$ MPa and a compressive yield strength of $R_{0.2} = 12.1 \pm 0.4$ MPa. The Young's Modulus of the lattice material was determined to be 763 ± 176 MPa. For comparison, bulk SLM titanium was mechanically characterized in tensile tests: $R_m = 662.1 \pm 20.6$ MPa, $R_{0.2} = 555.2 \pm 19.4$ MPa, $E_0 = 119 \pm 13.7$ GPa (Table 2).

Bone formation

After the operation, no adverse reaction was observed and the animals remained in good health. For each implant, the volume of the entire implant and the volume of the bone grown into the implant and their ratio (bone volume/total volume) were determined based on μCT data reconstructed to a 3D model (Fig. 3). The mean value of the volume of bone related to the entire volume of the implant determined by μCT accounted for 10.46% ± 1.95% for the empty control, 19.23% ± 6.39% for the native SLM implant, 25.23% ± 7.82% for sandblasted SLM implants, and 14.81% ± 1.74% for sandblasted and acid-etched SLM implants. These μCT results were not significantly different between the empty control and the three different surface modifications of SLM implants. The lattice structures used here proved not to be suitable for tomographic investigations, as they exhibit a large surface/solid ratio with huge interface scattering. Therefore, the distribution of newly formed bone was studied based on the ground sections.

In the ground sections, no signs of inflammation could be detected. Bone formation occurred close to and in contact with the bone substitutes (Figs. 4 and 5), which indicates a good biocompatibility over the first 8 weeks on implantation

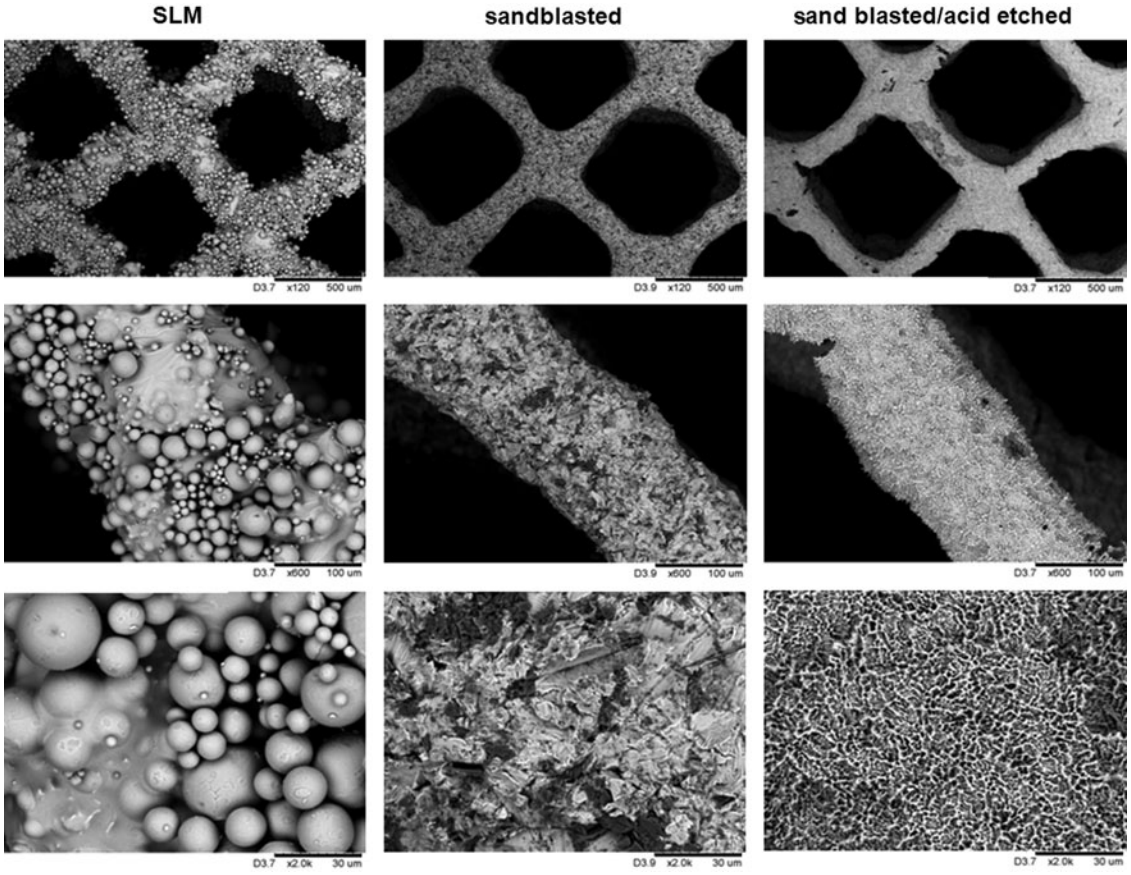

FIG. 2. Surface characterization of the implants. Scanning electron microscopy images of native SLM (left column), sandblasted SLM (middle column), and sandblasted and acid-etched surfaces (right column). Scales provided from upper to lower images are: 500, 100, and 30 μm.

for all SLM implants irrespective of the surface treatment. The histomorphometric analysis of the middle section given in mean number of bone points was 44.40 ± 14.88 points in the empty control samples, 128 ± 49.09 points for SLM implants, 174.20 ± 63.92 points for sandblasted SLM, and 175.20 ± 75.97 points for sandblasted and acid-etched SLM implants. The number of bone points falling on mineralized bone in the defect in all groups with implants was significantly higher ($p = 0.043$) than in the control group where no implant was placed. Between the groups with implants, the number of bone points was not significantly different, irrespective of the surface treatment.

By dividing the middle section in an area of presumably resected bone and an area outside of the original bone margins, it appeared that bone formation beyond the original bone margins was facilitated by the presence of this implant type (Fig. 6a). Bone formation in the control group without implant was almost exclusively restricted to the original bone area (Fig. 6b). In all groups with implants, significantly ($p = 0.043$) more bone formed compared with the control group in both the area outside the original bone margins and the area of the resected bone, irrespective of the surface treatment (Fig. 6). In the presumably original bone margins, significantly ($p = 0.043$) more bone formed in sandblasted than in untreated SLM implants.

Another way to look at the distribution of newly formed bone is to assess the percentage of defect bridging. Based on the histology of the middle sections, the untreated defects exhibit defect bridging of 56.67% ± 23.13%, SLM of 78.33% ± 26.09%, sandblasted SLM of 86.67% ± 13.94%, and sandblasted and acid-etched SLM of 96.67% ± 7.46%, respectively. Compared with untreated defects, the increase in defect bridging by bone is significant for the sandblasted and acid-etched implants only ($p = 0.043$) (Fig. 7).

Table 2. Mechanical Characterization of Selective Laser Melting Bar and Scaffold

Sample	*Porosity [%]*	$R_{0.2}$ *[MPa]*	*E [MPa]*	R_m *[MPa]*	*Pore size [mm]*
SLM Ti scaffold	83.5	12.1 ± 0.4	0.7 ± 0.2	15.9 ± 0.4	0.7
SLM Ti bar	0	555.0 ± 19.4	119.0 ± 13.7	662.9 ± 20.6	0.0

Discussion

In this study, open porous titanium structures were prepared by AM and placed in the calvaria of New Zealand rabbits. The lattice was defined with orthogonal struts of 200 μm thickness and a pore size of 700 μm width. The

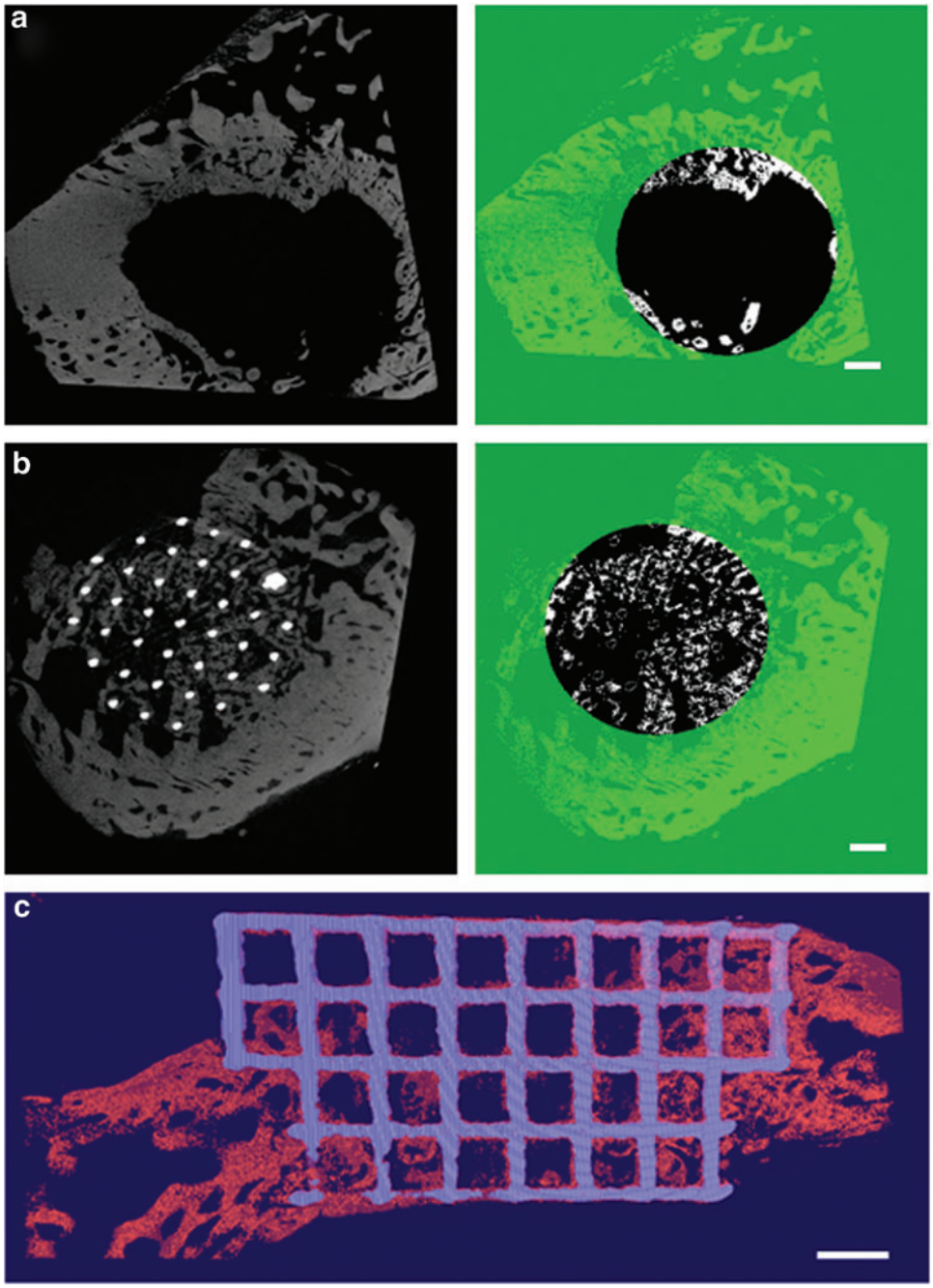

FIG. 3. μCT reconstruction. **(a)** μCT image (left) and the reconstructed bone (right) of an empty and **(b)** a defect treated with a SLM sandblasted implant are shown as representative examples. The white regions (right) show the identified bone area within the ROI after density segmentation. **(c)** 3D visualization of a transversal section with a thickness of 60 μm of the 3D data set from the same implant as in **(b)** with sandblasted surface: The bone appears red, and the titanium implant appears blue. Scale bars indicate 1 mm. 3D, three-dimensional; μCT, micro computed tomography. Color images available online at www.liebertpub.com/tea

thickness of the native implants produced by SLM, however, are thicker due to spherical powder particles that are sintered onto the solid surface (Fig. 2). The emerging cavities, therefore, are smaller than designed. By sandblasting, the decorating particles are removed (see Fig. 2), the wall thickness is reduced, and the cavities become larger. It is important to note that the final implant geometry is dependent on the CAD model geometry, the SLM processing parameter, and the successive surface treatment. The laser parameters can be adjusted in order to compensate for these facts. It is known that the pore dimensions used here (578 μm, resp. 642 μm) allow good osseointegration and vascularization in metallic[29] and ceramic foams.[30,31]

The scaffolds were mechanically characterized in an axial biomechanical loading case simulating pressure on the scaffold in the calvaria (Table 2). The static compression tests showed that the mechanical strength of this scaffold is in the upper range of cancellous bone, Therefore, this scaffold could substitute for the use of cancellous autologous bone.[32]

All implants showed good *in-vivo* performance with mineralized bone and no indication of adverse tissue reactions (Figs. 4 and 5). For all three types of implants, the amount of bone within the implant and around the implant was significantly higher than in the control group where no implant was placed (Fig. 6). Therefore, the titanium-based scaffolds stimulated additional bone formation and served as

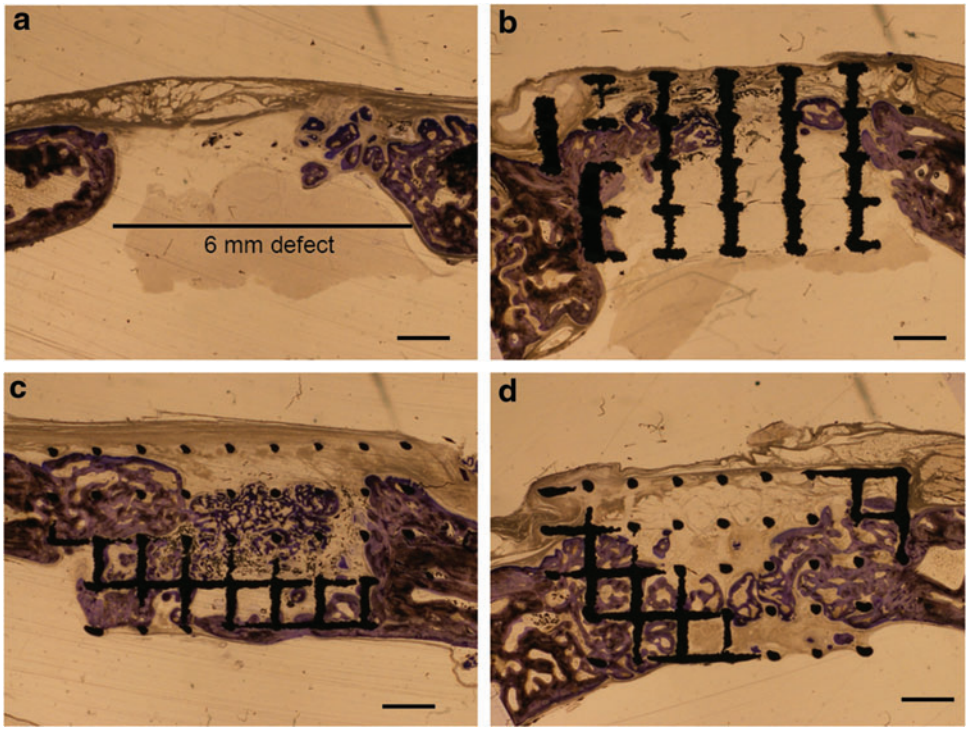

FIG. 4. Histological sections from the middle of the defect from one exemplary animal 8 weeks postoperatively. **(a)** Untreated defect (empty), **(b)** native SLM **(c)** sandblasted SLM, and **(d)** sandblasted and acid-etched surface. Scale bars indicate 1 mm. Original magnifications were 100-fold. Bone appears as grayish purple. The size of the original defect is indicated in **(a)**. Color images available online at www.liebertpub.com/tea

guidance cues even beyond the original bone margins. When the same model was used for calcium phosphate-based materials such as synthetic hydroxyapatite/silica oxide-based granules,[27] a cotton-wool-like nanocomposite,[33] synthetic calcium phosphate granules,[34] or deproteinized bovine mineral matrix granules,[27,28,33] overall bone formation was either not increased or the increase was not significant.

Defect bridging, another clinically relevant parameter, also failed to be increased for all aforementioned calcium phosphate-based materials when compared with untreated empty defects. The newly developed titanium-based scaffolds evaluated here, however, increased defect bridging significantly, at least when the surface was sandblasted and acid etched. The superior performance in the stimulation

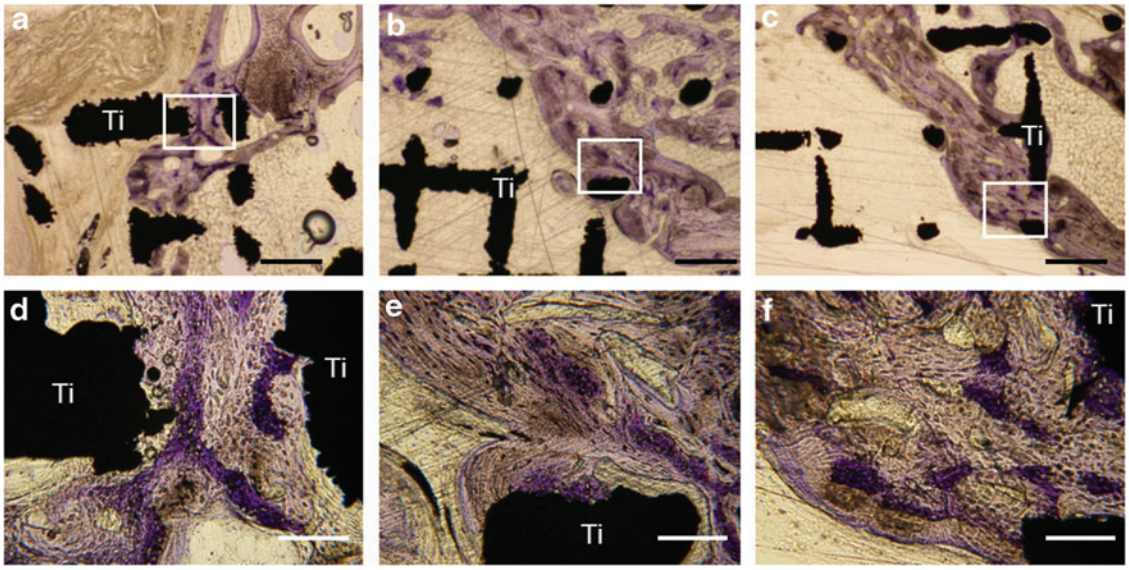

FIG. 5. High magnifications of histological sections from the middle of the defect 8 weeks postoperatively. **(a, d)** native SLM **(b, e)** sandblasted SLM and **(c, f)** sandblasted and acid-etched surface. The white square indicates the location of the related higher magnification picture in the lower panel. Black scale bars (upper panel) indicate 500 μm; white scale bars (lower panel) 100 μm. Original magnifications were 200 **(a–c)**-and 1000 **(d–f)**-fold. Titanium (black) is indicated by Ti. The grayish-stained bone tissue is lamellar bone (also new, but later formed) on the initial woven bone structures stained purple. Color images available online at www.liebertpub.com/tea

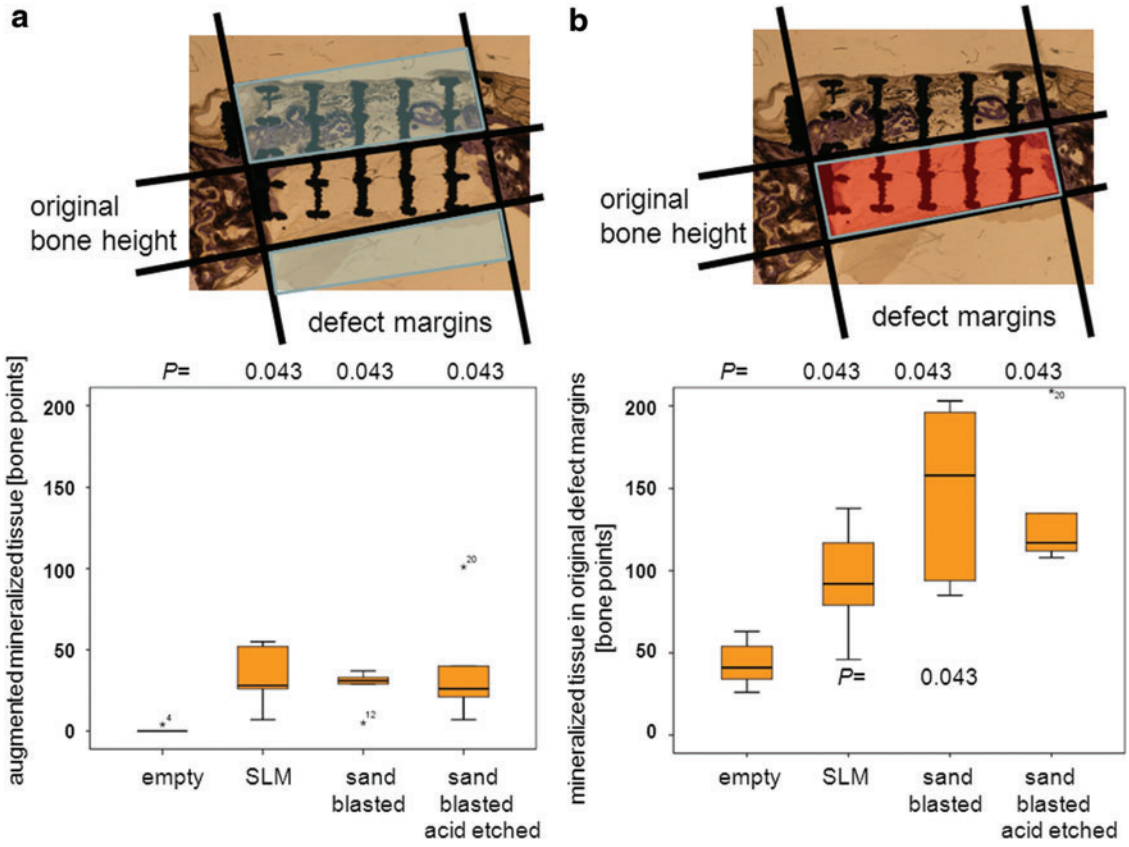

FIG. 6. Bone formation in and outside the original bone margins. **(a)** Bone formation beyond the original bone is significantly increased in all implant groups compared with the control group. An illustration of the region of bone formation beyond the original margins (blue area) is provided in the upper panel. **(b)** Bone formation in the original margins of the bone. Bone formation in the middle section is significantly increased with SLM implants, irrespective of their surface treatment compared with the control groups without implant. The area of the original bone margins (red) is illustrated in the upper panel. In the margins of the original bone, significantly more bone formed in the sandblasted SLM group compared with the native SLM group. Mineralization is given as number of grid points fallen on mineralized tissue in the defined area of interest (blue or red). Superscript numbers indicate individual data points outside the box. Color images available online at www.liebertpub.com/tea

of additional bone formation and defect bridging of our titanium-based scaffolds compared with deproteinized bovine bone matrix, the gold standard bone substitute in dentistry, and newly developed bone substitutes tested in the same setting[27,33,34] might arise from the minimal amount of material we used due to our scaffold design, the gapless interconnectivity throughout the whole scaffold, and/or the well-known excellent performance of titanium in a bone regeneration context.

A systemic review on surface roughness of titanium revealed that moderately rough surfaces with a roughness between 1.00–2.00 μm are superior to both smoother (0.50–1.00 μm) and rougher (>2.00 μm) surfaces.[35,36] Therefore, native SLM fabricated materials have to undergo a surface treatment such as sandblasting for an optimal performance in a bony environment. This was in line with our results, as significantly more mineralized tissue was formed in the original defect margins in sandblasted scaffolds with a roughness determined as arithmetic mean deviation of the surface (SRa) of 0.94±0.07 compared with native SLM scaffolds with an SRa value of 3.33±0.27 (Table 1, Fig. 6b).

It was already shown *in-vivo* that solid Ti6Al4V implants can be generatively manufactured by e-beam melting and

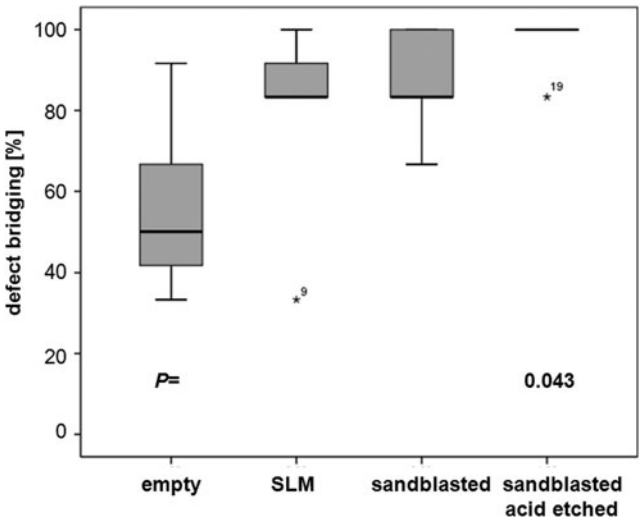

FIG. 7. Defect bridging is the percentage of the defect where new bone formation has occurred. Superscript numbers indicate individual data points outside the box.

that they are well integrated into rabbit femur and tibia after 6 weeks.[37] SLM was also used to produce experimental titanium-based rods with four nonconnected channels of different dimensions to study the relation between osteoconduction and channel dimension.[7] From the tested channels with a width between 500 and 1200 μm, osteoconduction in terms of bone formation in the more central part was best for the 500 μm channels. The pore size of interconnecting pores in our 3D scaffolds was between 578 and 642 μm and, therefore, close to the optimal values.

In addition, by SLM, a 3D-titanium-based scaffold was fabricated to resemble human cancellous bone.[38] In this case, the titanium struts were 400–800 μm thick and, therefore, much thicker than our regular-shaped scaffold with a strut size of 220 μm and the porosity varied from 55–75%. For our scaffolds with a porosity of 83%, as evident in Figure 4c, approximately 50% of the area of the middle section where the scaffold resided was filled with mineralized tissue. In terms of bone ingrowth, Pattanayak and co-workers found bone formation predominantly at the outer surface and only a very small fraction estimated to be below 5% inside the scaffold. This is evident from the histological illustrations.[38] Specific data on bone ingrowth and osteoconductivity were, however, not provided by these authors. In contrast, the present study demonstrates that our newly designed scaffolds aiming at a minimal amount of titanium by high porosity, minimal strut thickness, maximal interconnectivity of the pore-forming channels in the 550–650 μm range, and an optimized surface treatment are truly osteoconductive, surpass even calcium phosphate-based bone substitutes in this regard, and guide new bone formation throughout the entire scaffold.

The design of our scaffolds realized by SLM followed by a surface treatment allow a tight connection to the body and a reduced stress shielding due to its decreased stiffness, which matches the overall mechanical properties of cancellous bone. Therefore, it could serve as mechanically stable, osteoconductive scaffold to contain mechanically less stable osteoinductive materials such as hydrogels and/or cell constructs for bone tissue engineering purposes. For bone regeneration, as tested here, the osteoconductivity of our scaffolds is potent enough to guide new bone to be formed at sites outside the original bone margins, so that our scaffolds could prove useful not only as a bone substitute suitable for the treatment of substantial bone defects but also for challenging bone augmentation purposes in oral surgery and dentistry.

In conclusion, we designed and produced a titanium-based bone substitute by SLM to resemble mechanically and structurally cancellous bone as well as to avoid stress shielding. This in combination with a high porosity of 83% and a pore size of 500–600 μm led to a highly osteoconductive bone substitute. The *in vivo* results using SLM native, SLM sandblasted and SLM sandblasted, acid-etched compared with an empty defect revealed that overall bone formation increased significantly. Our results also showed that bone formed in the scaffold outside the original bone margins, and that sandblasted, acid-etched scaffolds showed a significant increase in defect bridging. In addition, we noticed that especially the treated SLM surface scaffolds show a superior osteoconductivity which facilitates more bone formation, and could be further developed for bone substitutes that are suitable for the reconstruction of large bony defects.

Acknowledgments

The authors would like to thank Alexandr Tchouboukov for technical assistance and the partial financial support rendered by AOCMF, the Cranio–Maxillofacial Specialty of the AO Foundation via the project (10-C-37W).

Disclosure Statement

No competing financial interests exist.

References

1. St-Pierre, J.P., Gauthier, M., Lefebvre, L.P., and Tabrizian, M. Three-dimensional growth of differentiating MC3T3-E1 pre-osteoblasts on porous titanium scaffolds. Biomaterials **26,** 7319, 2005.
2. Imwinkelried, T. Mechanical properties of open-pore titanium foam. J Biomed Mater Res A **81,** 964, 2007.
3. Levine, B.R., Sporer, S., Poggie, R.A., Della Valle, C.J., and Jacobs, J.J. Experimental and clinical performance of porous tantalum in orthopedic surgery. Biomaterials **27,** 4671, 2006.
4. Singh, R., Lee, P.D., Lindley, T.C., Kohlhauser, C., Hellmich, C., Bram, M., *et al.* Characterization of the deformation behavior of intermediate porosity interconnected Ti foams using micro-computed tomography and direct finite element modeling. Acta Biomater **6,** 2342, 2010.
5. Bansiddhi, A., Sargeant, T.D., Stupp, S.I., and Dunand, D.C. Porous NiTi for bone implants: a review. Acta Biomater **4,** 773, 2008.
6. Körner, C., and Singer, R.F. Processing of metal foams—challenges and opportunities. Adv Eng Mater **2,** 159, 2000.
7. Fukuda, A., Takemoto, M., Saito, T., Fujibayashi, S., Neo, M., Pattanayak, D.K., *et al.* Osteoinduction of porous Ti implants with a channel structure fabricated by selective laser melting. Acta Biomater **7,** 2327, 2011.
8. Mullen, L., Stamp, R.C., Fox, P., Jones, E., Ngo, C., and Sutcliffe, C.J. Selective laser melting: a unit cell approach for the manufacture of porous, titanium, bone in-growth constructs, suitable for orthopedic applications. II. Randomized structures. J Biomed Mater Res B Appl Biomater **92,** 178, 2010.
9. Murr, L.E., Quinones, S.A., Gaytan, S.M., Lopez, M.I., Rodela, A., Martinez, E.Y., *et al.* Microstructure and mechanical behavior of Ti-6Al-4V produced by rapid-layer manufacturing, for biomedical applications. J Mech Behav Biomed Mater **2,** 20, 2009.
10. Warnke, P.H., Douglas, T., Wollny, P., Sherry, E., Steiner, M., Galonska, S., *et al.* Rapid prototyping: porous titanium alloy scaffolds produced by selective laser melting for bone tissue engineering. Tissue Eng Part C Methods **15,** 115, 2009.
11. Meier, H., and Haberland, C. Fundamental studies on the influence of process parameters on the properties of SLM parts. Materialwissenschaft und Werkstofftechnik **93,** 665, 2008.
12. Weber, F.E., Eyrich, G., Gratz, K.W., Maly, F.E., and Sailer, H.F. Slow and continuous application of human recombinant bone morphogenetic protein via biodegradable poly (lactide-co-glycolide) foamspheres. Int J Oral Maxillofac Surg **31,** 60, 2002.
13. Li, J.P., de Wijn, J.R., van Blitterswijk, C.A., and de Groot, K. Porous Ti6Al4V scaffolds directly fabricated by 3D fibre

deposition technique: effect of nozzle diameter. J Mater Sci Mater Med **16,** 1159, 2005.
14. Zhao, G., Zinger, O., Schwartz, Z., Wieland, M., Landolt, D., and Boyan, B.D. Osteoblast-like cells are sensitive to submicron-scale surface structure. Clin Oral Implants Res **17,** 258, 2006.
15. Zhao, G., Raines, A.L., Wieland, M., Schwartz, Z., and Boyan, B.D. Requirement for both micron- and submicron scale structure for synergistic responses of osteoblasts to substrate surface energy and topography. Biomaterials **28,** 2821, 2007.
16. Schumacher, R., de Wild, M., Fabbri, S., Yildiz, A., and Schkommodau, E. Rapid manufacturing of individual Ti-6AI-4V bone implants. Eur Cell Mater **17,** 22, 2009.
17. Marx, R.E. Bone and bone graft healing. Oral Maxillofac Surg Clin North Am **19,** 455, 2007.
18. Brunette, D.M., Tengvall, P., and Textor, M. Titanium in Medicine: Material Science, Surface Science, Engineering, Biological Response and Medical Applications. Berlin: Springer, 2001.
19. Ferguson, S.J., Broggini, N., Wieland, M., de Wild, M., Rupp, F., Geis-Gerstorfer, J., *et al.* Biomechanical evaluation of the interfacial strength of a chemically modified sandblasted and acid-etched titanium surface. J Biomed Mater Res A **78,** 291, 2006.
20. Kasemo, B., and Gold, J. Implant surfaces and interface processes. Adv Dent Res **13,** 8, 1999.
21. Rupp, F., Scheideler, L., Olshanska, N., de Wild, M., Wieland, M., and Geis-Gerstorfer, J. Enhancing surface free energy and hydrophilicity through chemical modification of microstructured titanium implant surfaces. J Biomed Mater Res A **76,** 323, 2006.
22. Schuler, M., Kunzler, T.P., de Wild, M., Sprecher, C.M., Trentin, D., Brunette, D.M., *et al.* Fabrication of TiO2-coated epoxy replicas with identical dual-type surface topographies used in cell culture assays. J Biomed Mater Res A **88,** 12, 2009.
23. Kieswetter, K., Schwartz, Z., Hummert, T.W., Cochran, D.L., Simpson, J., Dean, D.D., *et al.* Surface roughness modulates the local production of growth factors and cytokines by osteoblast-like MG-63 cells. J Biomed Mater Res **32,** 55, 1996.
24. Bornstein, M.M., Lussi, A., Schmid, B., Belser, U.C., and Buser, D. Early loading of nonsubmerged titanium implants with a sandblasted and acid-etched (SLA) surface: 3-year results of a prospective study in partially edentulous patients. Int J Oral Maxillofac Implants **18,** 659, 2003.
25. Buser, D., Broggini, N., Wieland, M., Schenk, R.K., Denzer, A.J., Cochran, D.L., *et al.* Enhanced bone apposition to a chemically modified SLA titanium surface. J Dent Res **83,** 529, 2004.
26. de Wild, M., Maier, K., Schneider, M., Tschumi, S., and Schumacher, R., Albrecht, H. Surface modification and *in-vitro* investigation of generatively produced implants. BIOmaterialien **11,** 157, 2010.
27. Kruse, A., Jung, R.E., Nicholls, F., Zwahlen, R.A., Hammerle, C.H., and Weber, F.E. Bone regeneration in the presence of a synthetic hydroxyapatite/silica oxide-based and a xenogenic hydroxyapatite-based bone substitute material. Clin Oral Implants Res **22,** 506, 2011.
28. Schmidlin, P.R., Tchouboukov, A., Wegehaupt, F.J., and Weber, F.E. Effect of cerium chloride application on fibroblast and osteoblast proliferation and differentiation. Arch Oral Biol **57,** 892, 2012.
29. Bobyn, J.D., Stackpool, G.J., Hacking, S.A., Tanzer, M., and Krygier, J.J. Characteristics of bone ingrowth and interface mechanics of a new porous tantalum biomaterial. J Bone Joint Surg Br **81B,** 907, 1999.
30. Jensen, S.S., Yeo, A., Dard, M., Hunziker, E., Schenk, R., and Buser, D. Evaluation of a novel biphasic calcium phosphate in standardized bone defects: a histologic and histomorphometric study in the mandibles of minipigs. Clin Oral Implants Res **18,** 752, 2007.
31. Malmstrom, J., Adolfsson, E., Arvidsson, A., and Thomsen, P. Bone response inside free-form fabricated macroporous hydroxyapatite scaffolds with and without an open microporosity. Clin Implant Dent Relat Res **9,** 79, 2007.
32. Wintermantel, E., and Ha, S.-W. Medizintechnik—Life Science Engineering. Berlin, Heidelberg: Springer-Verlag, 2009.
33. Schneider, O.D., Weber, F., Brunner, T.J., Loher, S., Ehrbar, M., Schmidlin, P.R., *et al. In vivo* and *in vitro* evaluation of flexible, cottonwool-like nanocomposites as bone substitute material for complex defects. Acta Biomater **5,** 1775, 2009.
34. Schmidlin, P.R., Nicholls, F., Kruse, A., Zwahlen, R.A., and Weber, F.E. Evaluation of moldable, *in situ* hardening calcium phosphate bone graft substitutes. Clin Oral Implants Res **24,** 149, 2013.
35. Wennerberg, A., and Albrektsson, T. Effects of titanium surface topography on bone integration: a systematic review. Clin Oral Implants Res **20 Suppl 4,** 172, 2009.
36. Wennerberg, A., and Albrektsson, T. On implant surfaces: a review of current knowledge and opinions. Int J Oral Maxillofac Implants **25,** 63, 2010.
37. Thomsen, P., Malmstrom, J., Emanuelsson, L., Rene, M., and Snis, A. Electron beam-melted, free-form-fabricated titanium alloy implants: Material surface characterization and early bone response in rabbits. J Biomed Mater Res B Appl Biomater **90,** 35, 2009.
38. Pattanayak, D.K., Fukuda, A., Matsushita, T., Takemoto, M., Fujibayashi, S., Sasaki, K., *et al.* Bioactive Ti metal analogous to human cancellous bone: Fabrication by selective laser melting and chemical treatments. Acta Biomater **7,** 1398, 2011.

Address correspondence to:
Franz E. Weber, PhD
Division of Cranio-Maxillofacial and Oral Surgery
Oral Biotechnology & Bioengineering
University Hospital
Frauenklinikstrasse 24
8091 Zürich
Switzerland

E-mail: franz.weber@zzm.uzh.ch

Received: December 20, 2012
Accepted: June 20, 2013
Online Publication Date: September 18, 2013